THE JOURNAL OF PHYSICAL CHEMISTRY A

 VOLUME 108, NUMBER 30, JULY 29, 2004

ARTICLES

Dissociation Dynamics of Difluoroacetic Acid from the Ground and Excited Electronic States

Awadhesh Kumar,* Hari P. Upadhyaya, and Prakash D. Naik

Radiation Chemistry and Chemical Dynamics Division, Bhabha Atomic Research Centre, Mumbai-400 085, India

Received: March 22, 2004; In Final Form: May 10, 2004

The photodissociation dynamics of difluoroacetic acid (DFA) is investigated in both its ground and the first excited electronic states employing, respectively, pulsed CO_2 and ArF (193 nm) lasers. DFA undergoes facile infrared multiphoton dissociation (IRMPD) on irradiation with a pulsed CO_2 laser to open up various dissociation channels from the ground electronic state. Energetically the most preferred primary dissociation channel of DFA is 1,3-HF elimination, as demonstrated by ab initio molecular orbital (MO) calculations and the unimolecular rates for all molecular channels using Rice−Ramsperger−Kassel−Marcus theory. Contrary to an assumed dissociation mechanism for fluorinated carboxylic acids, the decarboxylation reaction is observed as a primary dissociation channel in the IRMPD of DFA. The vibrationally excited photoproducts CO, CO_2, COFH, and HF have been detected by measurement of time-resolved infrared fluorescence. Photoexcitation of DFA to the electronically excited S_1 state at 193 nm leads to the cleavage of the C−OH bond—a higher energy channel absent in IRMPD—producing OH(v,J), which was detected state-selectively employing the laser-induced fluorescence technique. We measured partitioning of the available energy, and observed that the nascent OH(v,J) is generated vibrationally cold (i.e., in $v = 0$) with moderate rotational excitation (T_R = 630 ± 80 K). But, a high fraction of energy goes to the relative translation (f_T value of 0.37) of the photofragments. This observation is explained on the basis of the presence of an exit barrier for the C−OH bond cleavage reaction, and supported by modeling of the measured partitioning of energy and ab initio MO calculations. The transition-state structure for the C−OH bond cleavage producing OH could be calculated in the electronically excited state, T_1.

1. Introduction

Studies on fluoroacetic acids (FAAs) have attracted quite a bit of attention due to their atmospheric relevance. Trifluoroacetic acid (TFA) is the end product of the atmospheric degradation of hydrochlorofluorocarbons (HCFCs), CF_3CX_2H, where X = H, F, or Cl, the environmentally friendly alternative to chlorofluorocarbons (CFCs). Since TFA is metabolized by soil bacteria, after it is drained out of the atmosphere, to form monofluoroacetic acid (MFA), it is of significance to understand removal of these acids through decomposition to assess their impact on the environment.

There exists a long-standing interest in the dissociation dynamics of FAA.[1−9] The replacement of nonacidic H atoms in acetic acid by F atoms radically alters the mode of thermal decomposition of FAA, particularly with respect to decarboxylation and dehydration channels. For example, direct decarboxylation and dehydration channels, observed in the thermal

* To whom correspondence should be addressed. E-mail: awadesh@apsara.barc.ernet.in.

10.1021/jp048744c CCC: $27.50
Published on Web 07/02/2004

decomposition of acetic acid, are stated to be absent or unimportant in all three FAAs, i.e., TFA,[1−6] difluoroacetic acid (DFA),[7] and MFA.[8] The primary dissociation channel of FAA is assumed to be HF elimination in all these studies. In the dissociation induced through infrared multiphoton excitation (IRMPE), a molecule can have different dissociation channels, or the same channels as in the thermal dissociation but with a different distribution of the products. This difference results mainly because of the absence of surface effects and the high vibrational temperature in IRMPE. In IRMPE, a molecule is excited selectively to higher vibrational levels from which it dissociates without undergoing thermal equilibration, thereby implying a high vibrational temperature (T_V). Results on the infrared multiphoton dissociation (IRMPD) of TFA have been explained without involving direct decarboxylation and dehydration channels,[6] which is similar to its thermal dissociation.[1] However, the theoretical calculations indicate that the direct decarboxylation is an important dissociation pathway for TFA.[9] Does this disparity between the experimental results and the theoretical predictions of the dissociation pathways with respect to decarboxylation exist for other FAAs, such as DFA and MFA, also? Thus, to address this problem, we investigated dissociation pathways of DFA from its ground electronic state, both experimentally employing IRMPD and theoretically using ab initio molecular orbital theory. In addition, unlike TFA, this molecule offers an opportunity to explore the feasibility of the dehydration channel, which is stated to be absent in FAA. It will be interesting to investigate whether the dehydration channel is absent or unimportant in IRMPD of DFA. Further, photodissociation of DFA at 193 nm was also studied to compare the dynamics of dissociation of DFA on the ground potential energy surface (PES) with that on the excited PES. Recently, UV photodissociation of carboxylic acids,[10−21] in general, has acquired importance because it generates OH, the radical scavenger of the atmosphere. The laser at 193 nm excites the $n_O(C{=}O)-\pi^*(C{=}O)$ transition in carboxylic acids. Is the dynamics of dissociation leading to OH formation in DFA affected by F atoms, carriers of additional nonbonding electrons?

In the present work, multiple dissociation channels and the vibrationally excited photoproducts in the IRMPD of DFA are investigated. Time-resolved infrared fluorescence (IRF) is employed to detect vibrationally excited transient products. The dynamics of dissociation of DFA at 193 nm was probed by detecting the nascent OH product employing the laser-induced fluorescence (LIF) technique. The partitioning of the available energy into various degrees of freedom of products was measured, and theoretically modeled. The activation barrier and the enthalpy of reaction are evaluated using ab initio molecular orbital theory. We employed Rice−Rampsperger−Kassel−Marcus (RRKM) unimolecular theory to estimate the relative rate coefficients of the competing dissociation channels from the ground electronic state of DFA.

2. Experimental Section

The IRMPD of DFA with the 9R(24) line of a grating tuned pulsed CO_2 laser (Lambda Physik, EMG 201) was carried out in a stainless steel cell equipped with two pairs of KCl/BaF_2 windows. The laser was tightly focused in the center of the reaction cell with a Ge lens ($f = 10$ cm). For the stable product analysis, irradiation of DFA (∼1.0 Torr) was carried out in a static condition with about 200 laser pulses. The products were analyzed using an FT-IR spectrometer (Magna-IR 550, Nicolet) and a homemade gas chromatograph.

The time-resolved IRF experiments were performed under slow-flow conditions (with a steady pressure of about 1.0 Torr) to avoid effects of the accumulation of products. The pressure was measured by a capacitance manometer (MKS Baratron). The IRF observed was negligibly small when DFA was irradiated by the unfocused laser beam having a low fluence (∼0.25 J cm^{-2}). Hence, all IRF experiments were performed using a tightly focused beam (energy ∼250 mJ/pulse) using a Ge lens ($f = 10$ cm). The apparatus for time-resolved IRF experiments is described elsewhere[22] in detail. Briefly, the IRF produced by CO_2 laser photolysis was detected at the right angle geometry by a liquid N_2 cooled InSb detector (J-10D, Judson or IS-2.00, Graseby) equipped with a matched preamplifier. The output signal was fed to a LeCroy (9350A) digital oscilloscope for digitization, averaging, and background subtraction. The temporal profile of the IRF was stored in an IBM PC compatible floppy diskette for further data processing. The IRF spectra were obtained by using a circular variable filter (CVF, OCLI 902) with a band-pass (fwhm) of about 100 cm^{-1}. With CVF the IRF was greatly reduced, and hence cutoff IR filters (CVI 5800 or 5794) were employed to select fluorescence at wavelengths either <4.0 or >5.0 μm.

UV photolysis of DFA in a flow system was performed using an ArF laser at 193 nm. The nascent OH fragment was probed state-selectively using the LIF technique by exciting the (0,0) band of the $A\,^2\Sigma-X\,^2\Pi$ system of OH and monitoring the total A−X fluorescence. The experimental setup for the laser photolysis−laser-induced fluorescence (LP−LIF) is described elsewhere.[10] Briefly, we employed an excimer laser (Lambda Physik, Compex-102) operating at 193 nm as the photolysis laser and the second harmonic output of a dye laser (Quantel, TDL90) pumped by a seeded Nd:YAG laser (Quantel, YG980 E-20) at 532 nm as the probe beam. The dye laser operated with DCM special dye with a fundamental wavelength tuning range of 600−640 nm. The photolysis and the probe laser beams traversed orthogonally through two pairs of MgF_2 and quartz windows to intersect at the center of the stainless steel reaction chamber. The fluorescence was collected perpendicular to both the beams with a lens ($f = 50$ mm), and detected with a PMT. We employed a broad band-pass filter ($\lambda_{center} = 310$ nm, fwhm $= 20$ nm) to cut off the scattered light from the photolysis laser. Subsequently, the integrated fluorescence signal after averaging for 30 shots by a boxcar (SRS 250) was fed to a Pentium II PC, which controlled the scan. The time delay (∼50 ns) between the photolysis and the probe lasers was controlled by a digital delay generator.

The DFA vapor flowed through the reaction chamber with a static pressure of ∼100 mTorr, which was measured using a capacitance gauge (Pfeiffer Vacuum). We employed unfocused laser beams with substantially decreased energies to avoid any multiphoton process and saturation by the photolysis and the probe lasers, respectively. In our experimental conditions the LIF intensity depended almost linearly on the pressure of DFA, implying a negligible contribution to the OH yield from the photodissociation of the dimer of DFA.

The DFA (Aldrich, 98%) sample was thoroughly degassed with several freeze−pump−thaw cycles before flowing in the photolysis cell.

3. Theoretical Calculations

Ab initio molecular orbital (MO) calculations were performed with the Gaussian 92[23] program to investigate the PESs for various dissociation channels in the ground state and the OH channel in the excited electronic states of DFA accessible by 193 nm excitation. The geometries of the ground electronic state of DFA, various products, and the transition-state (TS) structures

were optimized with the B3LYP theory, which uses Becke's three-parameter hybrid exchange functional with the correlational functional of Lee, Yang, and Parr, using 6-311G(d,p) basis sets. The energies corresponding to the optimized geometries were calculated using the second-order Moller−Plesset (MP2) level of theory (in some cases at the coupled cluster singles and doubles, CCSD, level) with 6-311+G(d,p) basis sets. The harmonic vibrational frequencies and force constants were calculated to ensure that the stationary points on the potential energy surfaces are true saddle points. All transition-state structures are characterized by only one imaginary frequency and one negative eigenvalue of the force constant matrix.

Excited electronic state calculations were performed at the configuration interaction with single electronic excitation (CIS) level. Time-dependent density functional theory (TD-DFT)[24] with a 6-311+G(d,p) basis set was employed to calculate the vertical excitation energies of six low-lying electronic states. MOs were analyzed to assign each electronic transition. Each of the six excited-state geometries (S_1-S_3, T_1-T_3) was then fully optimized following the CIS method.

To understand the dynamics of the C−O bond cleavage leading to OH formation, potential energy (PE) curves were calculated as a function of the C−OH bond length. Since TD-DFT cannot optimize structures of excited states, we determined PE curves of all six excited states by constraining the geometry of DFA to the equilibrium position of the ground state with only the distance of the C−OH bond varied. We attempted to locate the TS structures for generation of OH on all probable electronic states to understand the PES responsible for OH.

4. Results and Analysis

4.1. Dissociation from the Ground Electronic State. *4.1.1. Stable Products*. The DFA sample (∼1.0 Torr) was irradiated with the 9R(24) line of a grating tuned TEA CO_2 laser in a static cell with BaF_2 windows. Four stable products, CO, CO_2, COFH, and CF_2H_2, were identified using a combination of gas chromatography (GC) and FT-IR absorption. Another photoproduct HF was identified by its IRF. When the IR absorption spectra of DFA were measured in a photolysis cell equipped with KCl windows instead of BaF_2, almost all the IR bands were shifted with altered intensities. In addition, the photodissociation yields of DFA were greatly reduced. These observations imply strong adsorption of DFA on the KCl windows. Hence, all the experiments were performed in a cell equipped with BaF_2 windows.

These observed stable products can originate from various dissociation channels of DFA. One of the commonly observed primary dissociation channels of a halogen-containing molecule is the molecular elimination of HX. Thus, unimolecular dissociation of vibrationally excited DFA, a multichannel system, is expected to produce a HF molecule via 1,1- or 1,3-elimination (reactions 1 and 2,

$$HF_2C-CO_2H \xrightarrow{(1,1)} FC-CO_2H + HF \quad (1)$$

$$\xrightarrow{(1,3)} HFC-CO_2 + HF \quad (2)$$

respectively), involving a three-centered or five-centered transition state, respectively. The relative importance of these channels can be estimated experimentally by real time detection of the carbene and the biradical, or by trapping these transient species. Alternatively, it can be investigated theoretically. We employed ab initio MO calculations to find the low-energy dissociation channels from the ground electronic state of DFA. Other primary molecular dissociation channels (reactions 3−5)

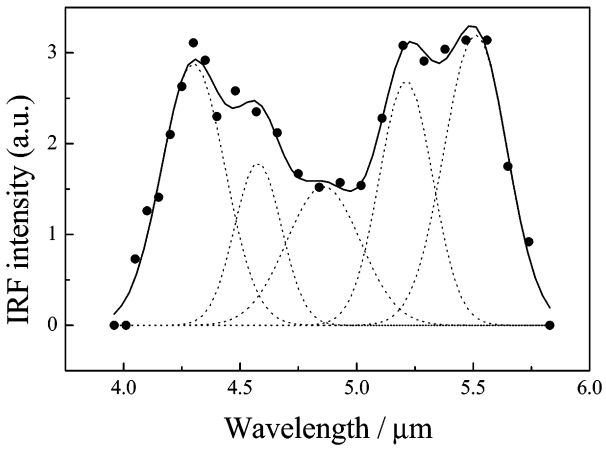

Figure 1. Infrared fluorescence spectra of the nascent photoproducts of DFA with a pulsed CO_2 laser at 8 μs after dissociation in slow-flow conditions at a steady pressure of ∼1.0 Torr. The solid curve represents the composite Gaussian function fit to the experimental points, and the dotted curves represent the deconvoluted IR emission bands at 4.3, 4.6, 4.9, 5.2, and 5.5 μm.

$$HF_2C-CO_2H \rightarrow H_2O + F_2C-CO \quad (3)$$

$$\rightarrow CO_2 + CF_2H_2 \quad (4)$$

$$\rightarrow HCO_2H + CF_2 \quad (5a)$$

$$\rightarrow FCO_2H + CFH \quad (5b)$$

are expected to be the elimination of H_2O (reaction 3), CO_2 (reaction 4), and HCO_2H or FCO_2H (reaction 5), after 1,2-migration of a H or F atom, respectively. Reaction 4 producing CF_2H_2, a greenhouse gas, is relevant to the atmospheric chemistry. In addition to the above-mentioned molecular pathways, dissociation of the vibrationally excited DFA can occur involving the radical channels, e.g., the C−C (reaction 6), the O−H (reaction 7), and the C−OH (reaction 8) bond ruptures.

$$HF_2C-CO_2H \rightarrow HF_2C + CO_2H \quad (6)$$

$$\rightarrow HF_2CCO_2 + H \quad (7)$$

$$\rightarrow HF_2CCO + OH \quad (8)$$

Detection of the stable products HF, CO_2, and CF_2H_2 in combination with our theoretical calculations (vide infra) implies that dissociation channels 1 and/or 2 and 4 are operative. The stable product CO can result from the transient species $FC-CO_2H$ (produced in reaction 1). The stable products CO, CO_2, and CF_2H_2 can also be formed as secondary products from radical channel 6, which is calculated theoretically to be a competing dissociation channel.

4.1.2. Measurement of Infrared Fluorescence. The available energy with the dissociating DFA can be partitioned among the various degrees of freedom of the photoproducts. We probed the vibrational excitation of the photoproducts with real time measurement of the IRF in a flow cell. The dispersed fluorescence spectrum peaking at ∼4.3 and ∼5.3 μm (shown in Figure 1) could be measured only when DFA underwent dissociation. This suggests that the observed fluorescence is mostly from the photoproducts. The observed spectrum in Figure 1 is deconvoluted into five Gaussian bands peaking at 4.3, 4.6, 4.9, 5.2, and

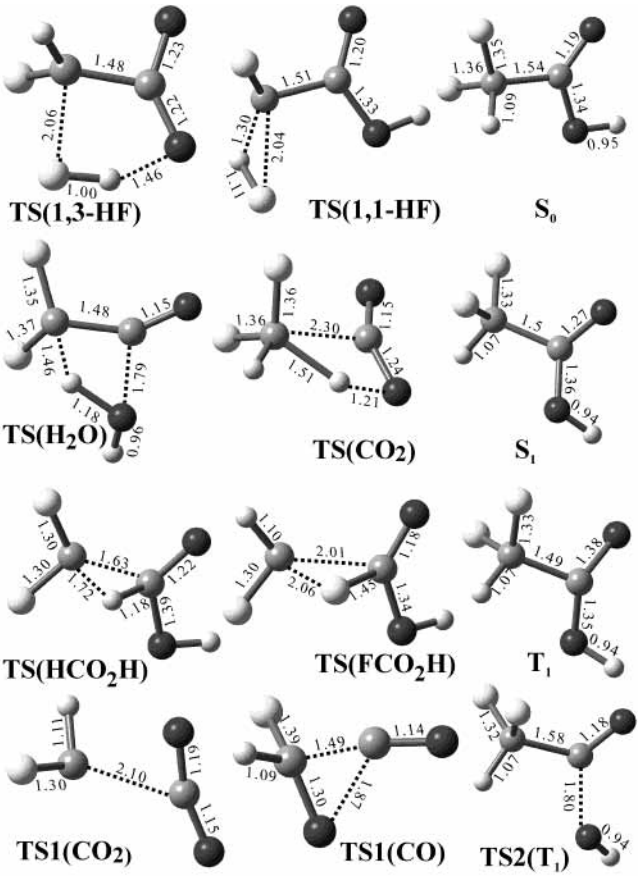

Figure 2. Optimized structures of the transition states for various molecular reactions from the ground electronic state of DFA, i.e., elimination of HF (both 1,1 and 1,3), H_2O, CO_2, HCO_2H, and FCO_2H (marked as TS below the structures), at the B3LYP level of theory using 6-311G(d,p) basis sets. Structures of the TSs (marked as TS1) of both CO_2 and CO elimination (reactions 9 and 10) from $HFCCO_2$ (a primary product of reaction 2) are depicted. The optimized structures of S_0, S_1, and T_1 of DFA along with the TS (marked as TS2) for OH formation after the C−O bond cleavage from the T_1 state are also shown in the last column. The breaking bonds are shown as dotted lines, and some important distances in angstroms are marked.

5.5 μm. The peaks at 4.3 and 4.6 μm are assigned to CO_2, those at 4.6 and 4.9 μm to CO, and those at 5.2 and 5.5 μm to COFH. The spectral bandwidth of the circular variable filter (CVF; OCLI) is too large ($\sim$100 cm^{-1}) to permit the measurements of the vibrational distributions of the nascent hot products observed, and with the CVF employed the fluorescence intensity was too small to measure the vibrational relaxation of the hot products. Therefore, IR filters were employed to measure the fluorescence at $<$4.0 μm, which is attributed mainly to the hot HF besides some other emitter(s), and that at $>$5.0 μm, assigned primarily to COFH.

4.1.3. Theoretical Results. The structures of DFA and the transition states of the molecular channels (reactions 1−5) are depicted in Figure 2. The figure displays structures of all four- and five-centered TSs to be planar or nearly planar. The relative energies for several dissociation channels are depicted in Table 1. To further support the relative importance of these molecular channels, we employed RRKM unimolecular theory,[25,26] using our theoretically calculated values of rotational constants, frequencies, and activation energies, to calculate rate coefficients at 148 kcal mol^{-1}. These calculated rate coefficients are also shown in Table 1.

Among various molecular and radical pathways of DFA, unlike those of TFA,[9] the lowest energy pathway is predicted

TABLE 1: Energies[a] of Different Transition States and Products, at the MP2/6-311+G(d,p) Level of Theory, Relative to the Reactant DFA with the RRKM Rate Coefficients of the Molecular Channels at 148 kcal mol^{-1}

dissociation channel of DFA yielding the products	transition state[b]	products[b]	RRKM rate coefficient (s^{-1})
Radical Channels			
$CF_2H + CO_2H$		+87.9 (83.8)	
$HF_2C\,CO + OH$		+106.2	
$HF_2C\,CO_2 + H$		+118.5	
Molecular Channels			
$FC\,CO_2H + HF$ (1,1-elimination)	80.4 (81.7)	+73.9	3.1×10^9
$FHC\,CO_2 + HF$ (1,3-elimination)	50.5 (55.1)	+31.8	1.2×10^{10}
$F_2C\,CO + H_2O$	84.0 (90.3)	+57.5 (57.2)	1.2×10^8
$CF_2H_2 + CO_2$	74.0 (81.2)	−16.3 (10.8)	1.3×10^9
$CF_2 + HCO_2H$	86.9 (87.6)	+59.1 (54.9)	7.6×10^7
$CFH + FCO_2H$	91.5 (90.2)	+82.9 (77.0)	2.1×10^7

[a] Kilocalories per mole. [b] Values in parentheses are at the CCSD/6-311+G(d,p) level of theory.

to be the 1,3-HF elimination (reaction 2) with an activation energy (E_a) of 55.1 kcal mol^{-1}. The 1,1-HF elimination (reaction 1, E_a = 81.7 kcal mol^{-1}) is the higher energy channel, implying that the five-centered TS (1,3-HF elimination) is more stable by 26.6 kcal mol^{-1} than the three-centered TS (1,1-elimination) for HF elimination from DFA. The high-energy HF elimination is in competition with other lower energy molecular pathways of CO_2 (reaction 4, E_a = 81.2 kcal mol^{-1}), HCO_2H (reaction 5a, E_a = 87.6 kcal mol^{-1}), FCO_2H (reaction 5b, E_a = 90.2 kcal mol^{-1}), and H_2O (reaction 3, E_a = 90.3 kcal mol^{-1}) elimination. The qualitative importance of these channels based on the calculated activation energies is supported by the RRKM prediction of the rate coefficients. The rate coefficient of the 1,3-HF elimination channel is predicted to be 3.9 times that of the 1,1-HF elimination channel at 148 kcal mol^{-1}. Although the difference between activation energies of these two HF elimination channels is 26.6 kcal mol^{-1}, their unimolecular rates are different by a factor of only 3.9. These low relative rates are mainly because of the relatively low vibrational frequencies and rotational constants of the TS corresponding to 1,1-HF elimination (the higher energy channel). Even the rate coefficient of the high-energy HF elimination channel is greater than that of the CO_2 and H_2O elimination channels by factors of 2.4 and 25.8, respectively. The H atom migration producing CF_2 and HCO_2H (reaction 5a) is preferred to the F atom migration (reaction 5b) by a factor of 3.6.

In earlier experimental works,[1−8] the 1,3-HF elimination is assumed to take place in dissociation of FAA to explain the stable products observed. Our ab initio theoretical calculations support this assumption, and suggest that the 1,3-HF elimination is the lowest energy dissociation pathway from the ground electronic pathway of DFA. The primary product $HFC-CO_2$ can have sufficient internal energy to undergo secondary dissociation, producing the molecular products CO_2 (reaction 9) and CO (reaction 10). TS structures for these two channels were calculated, and are given in Figure 2 (TS1(CO_2) and TS1(CO)). The channel leading to the CO product (E_a = 16.8 kcal mol^{-1}) is preferred to the CO_2 channel (E_a = 34.3 kcal mol^{-1}).

$$HFC-CO_2 \rightarrow CFH + CO_2 \quad (9)$$

$$\rightarrow COFH + CO \quad (10)$$

Thus, reaction 10 explains the observed product COFH. The effective E_a (assuming a similar frequency factor) for CO generation from DFA through reaction 10 (71.9 kcal mol^{-1}) being lower than that for CO_2 formation reaction 9 (89.4 kcal

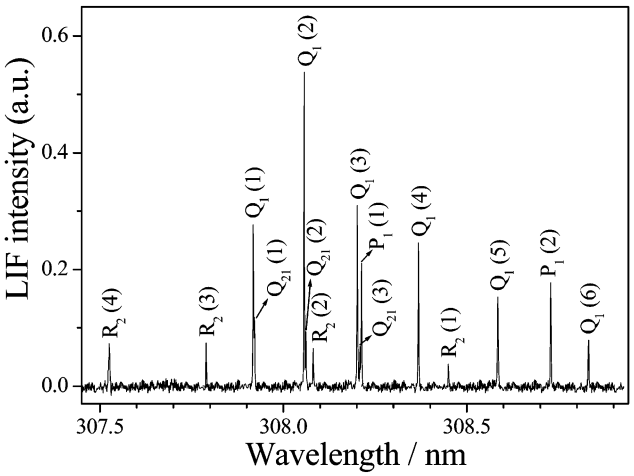

Figure 3. A portion of the fluorescence excitation spectra (at 50 ns delay) of the (0, 0) band of the A $^2\Sigma^+-$X $^2\Pi$ system of OH generated from photodissociation of difluoroacetic acid (~100 mTorr) at 193 nm.

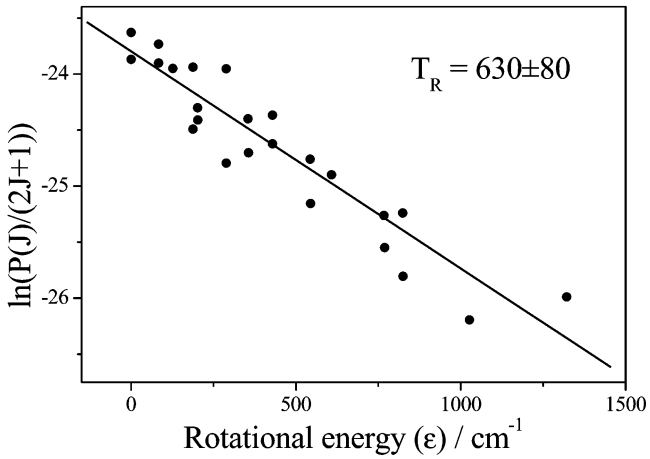

Figure 4. Boltzmann plot for rotational state distribution of OH (v = 0) with the rotational temperature, T_R = 630 ± 80 K.

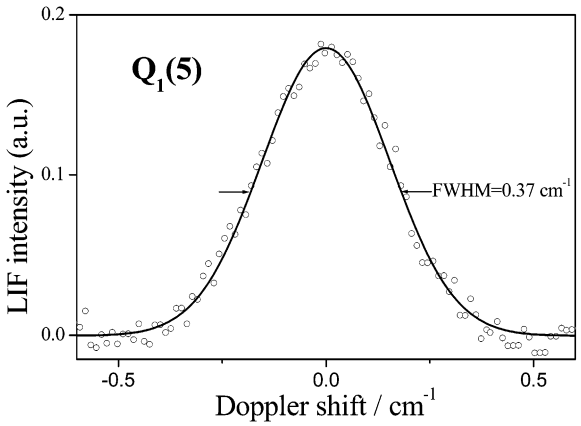

Figure 5. A typical Doppler-broadened $Q_1(5)$ line of the A $^2\Sigma^+-$X $^2\Pi$ (0, 0) system of OH, produced from irradiation of DFA at 193 nm.

mol^{-1}), the major fate of the coproduct biradical is to undergo dissociation, giving mainly CO and COFH. Although the frequency factor for reaction 9, which involves simple C−C bond cleavage, is expected to be higher than that for reaction 10, which involves a strained cyclic structure for the TS, it cannot offset the effect of the exponential energy factor of activation energy, and reaction 10 remains the preferred channel for the biradical. For the molecular channels involving the C−C bond cleavage (reaction 5) with simultaneous F and H atom migration in DFA, both channels are predicted to be almost equally probable energetically, with the latter having a small preference (Table 1).

4.2. Dissociation from an Excited Electronic State at 193 nm. DFA dissociates to produce the OH radical on excitation to the S_1 state via $n_O-\pi^*_{CO}$ transition at 193 nm. We measured the state distribution of OH to understand its dynamics of formation.

4.2.1. Nascent OH Distribution. The nascent photoproduct OH(v,J) was detected by LIF. Figure 3 shows the partial fluorescence excitation spectra of the (0, 0) band of the A $^2\Sigma^+-$X $^2\Pi$ system of OH. In assigning the line positions of OH, we use the standard notation $\Delta J(N)$ for the transition and denote transitions associated with the spin−orbit states X $^2\Pi_{3/2}$ and X $^2\Pi_{1/2}$ with subscripts "1" and "2", respectively. There is an insignificant vibrational excitation with most of the OH generated in the vibrational ground state. The average rotational and translational energies were determined using relative intensities and widths of lines, respectively.

4.2.1.1. Rotational and Translational Energy. The rotational lines of the (0, 0) band of OH were measured up to $N = 9$. The integrated area of each line was normalized with respect to the Einstein absorption coefficients (taken from ref 27) and energies of the photolysis and the probe lasers to extract information on the rotational temperature from the corrected relative intensities. The rotational population at J, $P(J)$, is proportional to the normalized line intensity, and is given by the Boltzmann equation

$$\ln(P(J)/(2J+1)) = -\epsilon hc/kT_R + \text{constant} \qquad (11)$$

The slope of eq 11 gives the rotational temperature, T_R = 630 ± 80 K (depicted in Figure 4). Only $P_1(N)$ and $P_2(N)$ rotational lines were used for calculating T_R, because these lines were mostly free from interference from other lines.

The average translational energy of the photoproduct OH was estimated using widths of Doppler-broadened rotational lines. The measured width was deconvoluted with the instrumental function (0.07 cm^{-1}), which was measured by the line width of thermalized OH at high pressure (50 Torr of ~0.1% DFA in He) and a longer delay time (110 μs). A typical Doppler-broadened line is shown in Figure 5. A few rotational lines were fitted to a Gaussian function, and their widths (fwhm), $\Delta\nu$, after deconvolution were used to calculate the translational temperature, T_T, using the Doppler relation

$$\Delta\nu = (7.16 \times 10^{-7})(T_T/m)^{1/2}\nu \qquad (12)$$

where m is the mass of the fragment OH. The average translational energy channeled into OH was estimated to be 12.9 kcal mol^{-1} from the average T_T.

4.2.1.2. Spin−Orbit and Λ-Doublet Population. The ground electronic state of OH being $^2\Pi$, there are two spin−orbit components, $^2\Pi_{3/2}$ and $^2\Pi_{1/2}$. The relative population, duly corrected, of $^2\Pi_{3/2}$ to $^2\Pi_{1/2}$ states of the product OH is plotted against N (depicted in Figure 6). The LIF intensities of only $P_{1,2}(N)$ lines are used to obtain the spin−orbit population. The figure shows the distribution of OH population in two spin−orbit states to be nonstatistical with a spin−orbit ratio $^2\Pi_{3/2}$/$^2\Pi_{1/2}$ of ~0.7; i.e., it has a small preference for $^2\Pi_{1/2}$. The deviation of the measured spin−orbit ratio cannot be ascribed to a difference in energies of the $^2\Pi_{3/2}$ and $^2\Pi_{1/2}$ states, as the latter is higher in energy. It can originate from the spin−orbit

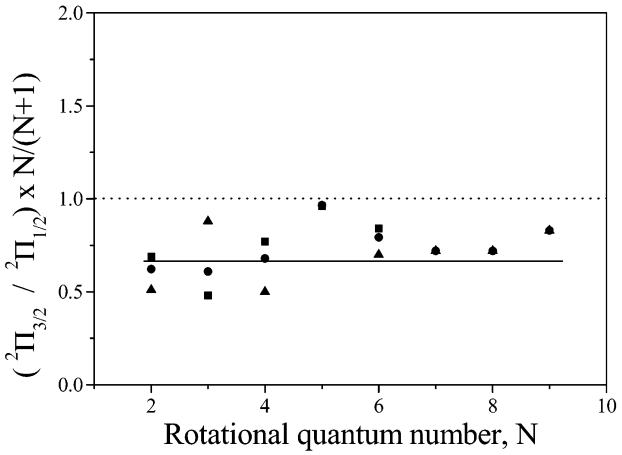

Figure 6. A plot of the relative populations of $^2\Pi_{3/2}$ to $^2\Pi_{1/2}$ states, after correction for different statistical weights, of the product OH against the rotational quantum number, *N*. Different data sets are plotted with different symbols.

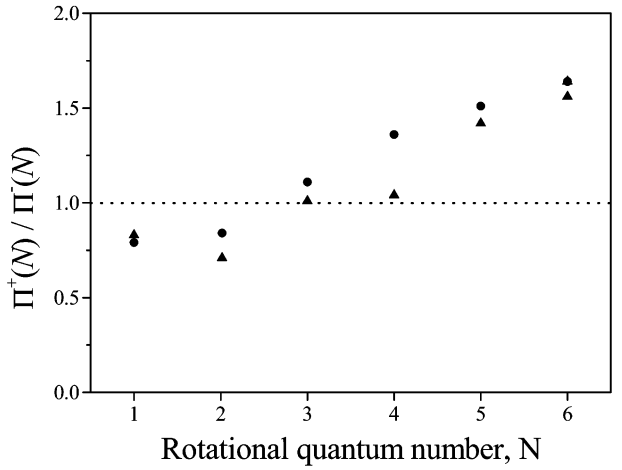

Figure 7. Λ-doublet ratio (Π^+/Π^-) of the product OH as a function of the rotational quantum number, *N*. Different data sets are plotted with different symbols.

interaction of the singlet with the nearby triplet state, or from inelastic scattering between the recoiling fragments.[28,29]

Each spin−orbit state of OH has two Λ-doublet components, denoted as Π^+ (or A′) and Π^- (or A″), depending on the orientation of the π lobe of the unpaired electron on OH with respect to the plane of rotation. In the high *J* limit, the Π^+ and Π^- Λ-doublets refer to the π lobe being in the plane or perpendicular to the plane of rotation, respectively. The population of the Π^+ and Π^- levels can be easily measured by probing the P- and R-rotational and Q-rotational lines, respectively. The Λ-doublet ratio depends on the process of generation of OH upon dissociation; that is, it gives information on the mechanism of dissociation. If the impulse is responsible for the dissociation process, OH rotates in the plane containing the dissociating C−OH bond axis due to in-plane dissociation. But if the torsional motion of the parent molecule plays a significant role upon dissociation, out-of-plane dissociation occurs. In Figure 7, we have plotted the Λ-doublet ratio (Π^+/Π^-), measured by the intensities of $P_1(N)$ and $Q_1(N)$ lines, as a function of *N*. The Λ-doublet states of OH ($X\ ^2\Pi_{3/2}$, $v = 0$), for $N = 1-6$, were found to be unequally populated, with the Λ-doublet population ratio Π^+/Π^- varying from 0.7 to 1.6 with *N*. Thus, the $^2\Pi^+$ levels are populated in preference to the $^2\Pi^-$ levels at higher *N*. This implies that mainly impulse upon dissociation is converted into rotation of products.

TABLE 2: Partitioning of the Available Energy,[a] Both Experimental and Theoretical, into Translation and Internal Modes of the Photofragments (OH and HF_2CCO) of Difluoroacetic Acid at 193 nm

	energy of the photofragment (kcal mol^{-1})			
type of energy	measured	statistical	impulsive	hybrid[b]
$\langle E_T(OH + HF_2CCO)\rangle$	15.6 ± 3.0	6.0	20.5	15.5
$\langle E_R(OH)\rangle$	1.2 ± 0.2	1.7	0.9	1.9
$\langle E_V(OH)\rangle$	0.0	0.7	0.1	0.2
$\langle E_{int}(HF_2CCO)\rangle$	25.0 ± 6.0	33.4	20.3	24.2

[a] $E_{avl} = 41.8$ kcal mol^{-1}. [b] With an exit barrier of 13.0 kcal mol^{-1}.

4.2.2. Product Energy Distribution. The available energy, E_{avl}, is the energy remaining after the dissociation to be partitioned between primary photoproducts. It is the sum of the photon energy and the internal energy of the parent molecule minus the bond dissociation energy. Thus, E_{avl} of the primary photoproducts OH and HF_2C-CO, $E_{avl}(OH + HF_2C-CO)$, can be expressed as

$$E_{avl}(OH + HF_2C-CO) = h\nu(193\ nm) + E_{int}(DFA) - D_0(HF_2C-CO-OH) \quad (13)$$

We estimated theoretically the bond dissociation energy $D_0(HF_2C-CO-OH)$ to be 106.2 kcal mol^{-1}. With the energy of the photon $h\nu$(193 nm) being 148.0 kcal mol^{-1} and after ignoring the small internal energy of the parent DFA molecules, the value of E_{avl} is estimated to be 41.8 kcal mol^{-1}. This energy is partitioned among various degrees of freedom between the photofragments with $E_{avl} = E_{int}(OH) + E_{int}(HF_2C-CO) + E_{trans}(OH + HF_2C-CO)$, where E_{int} consists of both the rotational and vibrational excitations. We estimated the average rotational energy of the OH fragment, $\langle E_{rot}\rangle$ to be 1.2 ± 0.2 kcal mol^{-1} after summing over the rotational excitation in the vibrational state populated ($v = 0$):

$$\langle E_{rot}\rangle = \sum P(J)\, E_{rot}(J) \quad (14)$$

where $P(J)$ is the state distribution and $E_{rot}(J)$ is the energy of a given rotational state *J* in $v = 0$. The average translational energy in OH is estimated from the Doppler profile to be 12.9 kcal mol^{-1}, which implies that the relative translational energy of the fragment pair, $\langle E_{trans}(OH + HF_2C-CO)\rangle$, is 15.6 kcal mol^{-1}. These measured data are summarized in Table 2. Thus, the remaining available energy of 25.0 kcal mol^{-1} is about 60% of the total energy, and is channeled into the internal energy of the coproduct HF_2C-CO.

4.2.3. Theoretical Results on Excited Electronic States. Each of the six excited electronic state geometries (S_1-S_3, T_1-T_3) was optimized following the CIS method. The optimized structure of the S_1 state (shown in Figure 2) has a nonplanar geometry for the carboxylic acid group in contrast to its almost planar geometry in the ground state. The major change in bond lengths is the extension of the C═O bond from 1.19 to 1.27 Å. The C−OH bond is also slightly extended from 1.34 to 1.36 Å. Thus, the structural changes coupled with analysis of molecular orbitals suggest $n_{O(C=O)}-\pi^*_{C=O}$ transition for the S_1 state. The lowest triplet state T_1 involves a transition similar to that of the S_1 state. But the C═O bond (1.38 Å) is extended more than that in S_1. The next higher triplet state T_2 has a mixed character involving $n_{O(C=O)}-\pi^*_{C=O}$ and $n_{O(OH)}-\pi^*_{C=O}$ transitions. Thus, as all the excited states of DFA accessible at 193 nm do not involve nonbonding electrons on F atoms, excitation of DFA is not affected due to the presence of F atoms.

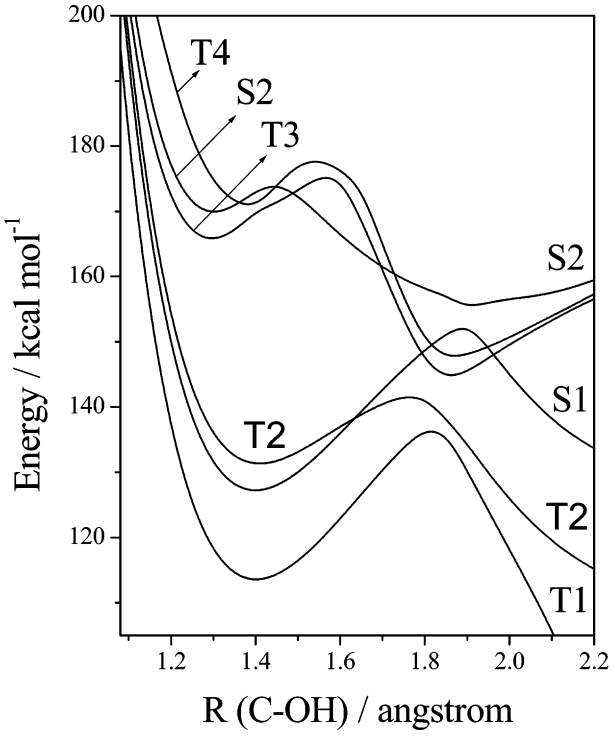

Figure 8. Potential energy curves for six lower excited electronic states of DFA calculated with the time-dependent B3LYP/6-311+G(d, p) method as a function of the C−OH bond length. The geometry was frozen to the equilibrium position of the ground state except for variation in the C−OH bond distance.

PE curves of the six low-lying excited states (S_1, S_2, T_1−T_4) are shown in Figure 8 as a function of the C−OH bond length, varied from 1.05 to 2.25 Å at intervals of 0.05 Å. All of these states of DFA are bound with respect to the C−OH bond. But the figure shows the distinct presence of exit barriers for the C−OH bond cleavage reaction from the S_1, T_1, and T_2 states. This implies that we should obtain the TS structures for the C−OH bond cleavage producing OH in the S_1, T_1, and T_2 states. We could characterize the TS structure, shown as TS2(T_1) in Figure 2, in the T_1 state using the CIS method. The TS is located 126 kcal mol^{-1} above the ground electronic state, implying that the exit barrier for the C−OH bond cleavage is ∼20 kcal mol^{-1}. Thus, initial excitation at 193 nm leads to population of DFA in the S_1 state, which relaxes to the lower state T_1 by nonradiative intersystem crossing. Subsequently, DFA dissociates from T_1 involving the C−O bond cleavage to generate OH.

5. Discussion

5.1. Dissociation Mechanism from the Ground Electronic State. Our studies reveal that the lowest energy primary dissociation channel from the ground electronic state of DFA is 1,3-HF elimination. The coproduct of HF, the biradical, in the 1,3-elimination reaction undergoes further dissociation to generate CO_2 and CFH (reaction 9) and CO and COFH (reaction 10). CO_2 is also a primary photoproduct generated involving a four-centered TS in reaction 4. This primary channel for CO_2 yield is expected to compete with the secondary source as it has a lower E_a of 81.2 kcal mol^{-1}. Whether CO is a primary product could not be answered as the corresponding TS was not found. The dehydration channel of DFA, whose TS structure was calculated with a high E_a of 90.3 kcal mol^{-1}, is not expected to compete with other low-energy channels and, hence, will be an insignificant reaction in the IRMPD of DFA.

The molecular products CO_2, CO, and COFH are formed involving cyclic TS structures. An appreciable amount of the exit barrier is expected to be partitioned to the relative translation of the photoproducts. Thus, only a small fraction of the available energy going to the internal states of the products is responsible for the IR fluorescence from CO_2, CO, and COFH. Although we could not resolve the distribution of energy over vibrational levels, only lower levels (mostly, $v = 1$) of these products are expected to be populated.

In addition to the molecular reaction channels, the C−C bond cleavage (reaction 6) among possible radical channels (reactions 6−8) can operate in the IRMPD of DFA. However, the other two high-energy channels, including the C−O bond cleavage giving OH, cannot operate from the ground electronic state of DFA. Such high-energy dissociation channels can open up from a higher electronic state on UV excitation. We detected the OH photoproduct on photoexcitation of DFA at 193 nm, and measured the state distribution of the nascent OH radical.

5.2. Dissociation from the Excited State: Energy Partitioning. A significant fraction (f_T value 0.37) of the available energy is transferred into the translational energy of the photofragments with a small fraction into the internal states of OH. The remaining energy is transferred into the internal states of the cofragment of OH, which implies an f_{INT}(cofragment) value of 0.60. Other measurements of f_T values involving the C−OH bond cleavage in acetic acid[10,21] and TFA[21] at 193 nm show similar results within experimental error. The average f_T value of 0.35 ± 0.06 and the f_{INT}(cofragment) value of 0.61 ± 0.07 for acetic acid and its fluoro derivatives at 193 nm suggest that the effect of fluorine substitution on energy partitioning is not significant.

A higher fraction of energy going to the relative translation implies either the impulsive dissociation of the HF_2CCO−OH bond or the presence of an exit barrier. As an impulsive dissociation occurs from a repulsive PES with a high dissociation rate coefficient, the observed results can be explained if the dissociative state of DFA is repulsive in nature. Our calculations (shown in Figure 8) suggest that the dissociative state is not repulsive. Thus, the impulsive dissociation of DFA is not responsible for the high relative translational energy in the products. The other plausible explanation, i.e., the presence of an exit barrier, can explain the observed results. An exit barrier to the C−O bond cleavage is observed for a simple bond cleavage leading to OH in photodissociation of acetic,[10,16] acrylic,[11] pyruvic,[12] and thiolactic[13] acids and, as expected, which has been subsequently substantiated by theoretical calculations,[14] in photodissociation of propiolic acid.[15]

The observed partitioning of the available energy among various degrees of freedom of the two photofragments can be examined considering two limiting models, the impulsive[30] and the statistical.[31] We employed both models to calculate partitioning of the available energy of 41.8 kcal mol^{-1} into various degrees of freedom of photofragments OH and HF_2C−CO. The structures of the ground and several excited electronic states of DFA along with the photofragments OH and HF_2C−CO were calculated using the Gaussian 92 program at the B3LYP/6-311+G(d,p) level. The statistical model assumes that all possible combinations of product states are equally probable under the constraint of conservation of energy. Our calculated vibrational frequencies and the rotational constants of the fragments were used to estimate the density of states. This model, results given in Table 2, underestimates the relative kinetic energy of the products, overestimates the internal energy of HF_2C−CO, and thus fails to explain the measured energy partitioned between

photofragments. The impulsive model is based on the assumption that the amount of available energy acts as a repulsive potential along the dissociating bond, i.e., the C−OH bond in DFA. Then, the energy partitioned between fragments is determined by conservation of linear and angular momenta. The impulsive model predicts partitioning of the available energy relatively closer to the experimental values (Table 2). However, the impulsive model cannot be responsible for the observed high translational energy in the fragments, because our calculations show (depicted in Figure 8) that none of the accessible excited states of DFA at 193 nm are repulsive in nature.

A nonsatisfactory explanation of partitioning of the available energy in the fragments by both the statistical and impulsive models prompted us to apply the hybrid model,[32,33] in which the E_{avl} for the products is divided into the excess energy above the transition state and the energy released by the exit barrier. Then partitioning of the excess and the exit barrier energies is treated, respectively, by the statistical and impulsive models. Contributions from each of these two models are added to obtain the energy in each fragment. The measured energy in the fragments is reproduced well with an exit barrier of 13.0 kcal mol^{-1}. The hybrid model of energy partitioning is supported qualitatively by calculation of the TS structure for the C−OH bond cleavage from the T_1 excited state of DFA. Although the fitted exit barrier (13.0 kcal mol^{-1}) of the hybrid model agrees reasonably well with our calculated value of ∼20 kcal mol^{-1}, we do not attach much importance to the quantitative agreement as the excited-state theoretical calculations are carried out at a low level of CIS theory. Thus, the origin of a barrier in the exit channel of the C−O bond cleavage of DFA is mainly due to nonadiabatic surface-crossing of the excited-state PESs.

Thus, like acetic acid, dissociation of DFA occurs from the T_1 state on excitation at 193 nm. Moreover, the energy partitioning between fragments is also almost similar within experimental error. The effect of fluorine substitution on the dynamics of dissociation is minimal, probably because of the fact that the lone pairs of electrons on F atoms of DFA are not involved in electronic transitions accessible at 193 nm. However, very recently we observed dissociation of thiolactic acid[13] at 193 nm taking place from the S_1, and not from the T_1, state. In this case, the lone pairs of electrons on the S atom are involved in the electronic transition to the S_1 state via $n_S-\pi^*_{C=O}$ transition, and thus, the dynamics of dissociation is affected by the SH chromophore.

6. Conclusions

Infrared multiphoton dissociation of DFA employing a pulsed CO_2 IR laser leads to the formation of the stable products CO, CO_2, COFH, CF_2H_2, and HF. Vibrationally excited CO, CO_2, COFH, and HF products are detected using time-resolved infrared fluorescence. Low-energy dissociation channels are examined theoretically using the ab initio MO and RRKM theories to calculate, respectively, the transition-state structures with energetics and unimolecular rates of the molecular channels. Both the detection of the stable products and theoretical calculations suggest that 1,3-HF elimination is energetically the most favorable channel from the ground electronic state of DFA, and decarboxylation reaction, a primary dissociation channel producing CF_2H_2 (a greenhouse gas), also takes place. Thus, the reactions of the OH radical with suitable carbonyl radicals producing vibrationally excited DFA in the atmosphere can lead to the production of the greenhouse gas CF_2H_2. On the basis of the high E_a as calculated, the dehydration reaction is expected to be an unimportant dissociation channel, and the C−OH bond cleavage producing OH to be absent. But, on excitation to the S_1 state at 193 nm, DFA undergoes C−OH bond cleavage, generating the OH radical, which is produced vibrationally cold with moderate rotational excitation. A significant fraction (∼40%) of the available energy is partitioned to the relative translation of the photofragments due to the presence of an exit barrier for the C−OH bond cleavage. Ab initio MO calculations for the excited states of DFA were performed to understand the origin of the exit barrier. Like carboxylic acids, which dissociate mostly from the T_1 state, DFA also dissociates from the T_1 state.

Acknowledgment. We acknowledge the courtesy of Dr. V. Parthasarathy for FT-IR analysis and Dr. T. Mukherjee for his constant encouragement throughout this work. A.K. acknowledges assistance from Prof. Y.-P. Lee, Taiwan, in some theoretical calculations.

References and Notes

(1) Blake, P. G.; Pritchard, H. *J. Chem. Soc. B* **1967**, 282.
(2) Pola, J. *Collect. Czech. Chem. Commun.* **1981**, *46*, 2854.
(3) Bischofberger, P.; Allemann, M.; Zwinselmon, J. J.; Kellerhals, H. *Spectrosc. Int. J.* **1984**, *3*, 50.
(4) Blake, P. G.; Shrayden, B. F. *Int. J. Chem. Kinet.* **1981**, *13*, 463.
(5) Simons, J. P.; Yarwood, A. J. *Nature* **1961**, *192*, 943.
(6) Kumar, A.; Vatsa, R. K.; Naik, P. D.; Rama Rao, K. V. S.; Mittal, J. P. *Chem. Phys. Lett.* **1993**, *208*, 385.
(7) Blake, P. G.; Pritchard, H.; Tomlinson, A. D. *J. Chem. Soc. B* **1971**, 607.
(8) Blake, P. G.; Tomlinson, A. D. *J. Chem. Soc. B* **1971**, 1596.
(9) Francisco, J. S. *J. Chem. Soc., Faraday Trans.* **1992**, *88*, 3521.
(10) Naik, P. D.; Upadhyaya, H. P.; Kumar, A.; Sapre, A. V.; Mittal, J. P. *Chem. Phys. Lett.* **2001**, *340*, 116.
(11) Upadhyaya, H. P.; Kumar, A.; Naik, P. D.; Sapre, A. V.; Mittal, J. P. *J. Chem. Phys.* **2002**, *117*, 10097.
(12) Dhanya, S.; Maity, D. K.; Upadhyaya, H. P.; Kumar, A.; Naik, P. D.; Saini, R. D. *J. Chem. Phys.* **2003**, *118*, 10093.
(13) Pushpa, K. K.; Upadhyaya, H. P.; Kumar, A.; Naik, P. D.; Bajaj, P. N.; Mittal, J. P. *J. Chem. Phys.* **2004**, *120*, 6964.
(14) Kumar, A.; Upadhyaya, H. P.; Naik, P. D. Unpublished work.
(15) Kumar, A.; Upadhyaya, H. P.; Naik, P. D.; Maity, D. K.; Mittal, J. P. *J. Phys. Chem. A* **2002**, *106*, 11847.
(16) Hunnicutt, S. S.; Waits, L. D.; Guest, J. A. *J. Phys. Chem.* **1991**, *95*, 562.
(17) Arendt, M. F.; Browning, P. W.; Butler, L. J. *J. Chem. Phys.* **1995**, *103*, 5877.
(18) Kitchen, D. C.; Forde, N. R.; Butler, L. J. *J. Phys. Chem. A* **1997**, *101*, 6603.
(19) Owrutsky, J. C.; Baronavski, A. P. *J. Chem. Phys.* **1999**, *111*, 7329.
(20) Su, H.; He, Y.; Kong, F.; Fang, W.; Liu, R. *J. Chem. Phys.* **2000**, *113*, 1891.
(21) Kwon, H. T.; Shin, S. K.; Kim, S. K.; Kim, H. L.; Park, C. R. *J. Phys. Chem. A* **2001**, *105*, 6775.
(22) Kumar, A.; Vatsa, R. K.; Naik, P. D.; Rama Rao, K. V. S.; Mittal, J. P. *Chem. Phys. Lett.* **1992**, *200*, 283.
(23) Frisch, M. J.; et al. *Gaussian 92*; Gaussian, Inc.: Pittsburgh, PA, 1992.
(24) These calculations were performed using Gaussian 98 in the laboratory of Prof. Y.-P. Lee, Taiwan.
(25) Gilbert, R. G.; Smith, S. C.; Jordan, M. J. T. UNIMOL program suite, 1993.
(26) Gilbert, R. G.; Smith, S. C. *Theory of Unimolecular and Recombination Reactions*; Blackwell Scientific Publications: Oxford and Cambridge, 1990.
(27) Chidsey, I. L.; Crosley, D. R. *J. Quant. Spectrosc. Radiat. Transfer* **1980**, *23*, 187.
(28) Goldsmith, J. E. M.; Kearsley, D. T. B. *Appl. Phys. B* **1990**, *50*, 371 and references therein.
(29) Naulin, C.; Costes, M.; Dorthe, G. *Chem. Phys. Lett.* **1988**, *143*, 496 and references therein.
(30) Tuck, A. F. *J. Chem. Soc., Faraday Trans. 2* **1977**, *73*, 689.
(31) Muckerman, J. T. *J. Phys. Chem.* **1989**, *93*, 179.
(32) North, S. W.; Blank, D. A.; Gezelter, J. D.; Longfellow, C. A.; Lee, Y.-T *J. Chem. Phys.* **1995**, *102*, 4447.
(33) Chang, A. H. H.; Hwang, D. W.; Yang, X.-M.; Mebel, A. M.; Lin, S. H.; Lee, Y.-T. *J. Chem. Phys.* **1999**, *110*, 10810.